ACS Biomaterials SCIENCE & ENGINEERING

pubs.acs.org/journal/abseba

Article

Mesenchymal Stem Cell Spheroids Embedded in an Injectable Thermosensitive Hydrogel: An In Situ Drug Formation Platform for Accelerated Wound Healing

Mohammad Ali Nilforoushzadeh, Mohsen Khodadadi Yazdi, Shaghayegh Baradaran Ghavami, Samila Farokhimanesh, Leila Mohammadi Amirabad, Payam Zarrintaj, Mohammad Reza Saeb, Michael R. Hamblin, Mehrak Zare,* and Masoud Mozafari*

Cite This: https://dx.doi.org/10.1021/acsbiomaterials.0c00988

Read Online

ACCESS | Metrics & More | Article Recommendations

ABSTRACT: The ability of mesenchymal stem cells (MSCs) to enhance cutaneous wound healing has been well established. Extensive expansion of cells to reach sufficient cell numbers for regenerating tissues has always limited cell-based therapies. An ingenious solution to address this challenge is to develop a strategy to increase the immunomodulatory effects of MSCs without expanding them. In this study, we employed a simple characteristic of cells. It was observed that an optimized three-dimensional (3D) MSC culture in spheroid forms significantly improved their paracrine effects. An electrospray (ES) encapsulation apparatus was used to encapsulate individual or 3D spheroid MSCs into microscale alginate beads (microbeads). Furthermore, alginate microbeads were embedded in an injectable thermosensitive hydrogel matrix, which gels at skin temperature. The hydrogel fills and seals the wounds cavities, maintains high humidity at the wound area, absorbs exudate, and fixes microbeads, protecting them from direct contact with the harsh wound environment. In vitro investigations revealed that secretion of interleukin 10 (IL-0) and transforming growth factor β1 (TGF-β1) gene was gradually enhanced, providing a delivery platform for prolonged release of bioactive molecules. In vivo study on full-thickness wounds showed granulation and re-epithelialization, only after 7 days. Moreover, increased expression of α-smooth muscle actin (α-SMA) in the first 14 days after treatment ensured wound contraction. Besides, a gradual decrease in α-SMA secretion resulted in reduced scar formation. Well-organized collagen fibrils and high expression of the angiogenesis biomarker CD31 confirmed the promoting effect of the hydrogel on the wound-healing process. The proposed wound-dressing system would potentially be used in scalable and effective cell-based wound therapies.

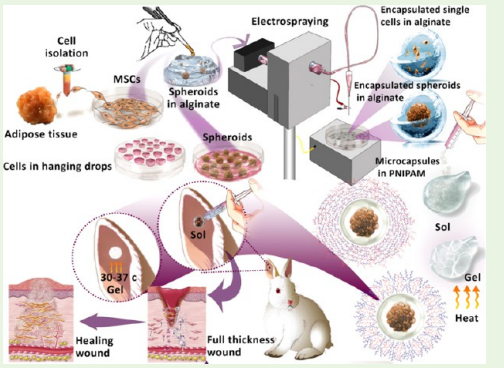

KEYWORDS: *skin wound healing, stem cells, cell delivery, injectable hydrogel, thermosensitive*

1. INTRODUCTION

Skin is the largest organ in the human body, which serves as the first-line protection against infection, disease, and dehydration. However, trauma, surgery, and special disease can result in skin wounds, which is a major healthcare problem. Normal wounds are usually healed through a four-phase process including hemostasis, inflammation, proliferation, and remodeling.[1] However, this natural process may be dysregulated resulting in nonhealing wounds. For a wound to heal successfully, all four phases must happen in the appropriate sequence and time frame and under balanced circumstances. Skin cells, extracellular matrix, and systemic factors comprise the main players in the wound-healing process. Any imbalances in these factors result in a nonhealing wound. The pathophysiology of wounds has indicated that nonhealing wounds could be due to diverse reasons.[2] Chronic wounds and burn injuries have long been a global health concern because they affect millions of people across the globe, annually.[3] Chronic wounds are created as a consequence of an abnormal skin wound repair process, resulting in growth confinement and movement disruption across joints and bear cosmetic and psychological problems to patients.[4−6]

Macrophages are key players of the inflammatory phase and transition from the inflammation to the proliferation phase. Polarization of macrophages to the M1 proinflammatory phenotype or the M2 anti-inflammatory phenotype significantly affects the wound fate.[7] Contrary to adult wounds, fetal

Received: July 4, 2020
Accepted: August 12, 2020

wound signaling is toward anti-inflammatory cytokines (M2 macrophage) and cells, resulting in complete regeneration.[8] Prolonged inflammation and reduced vascularization could be detrimental and may impede the healing/closure of wounds, resulting in more existence of T cells with a low CD4+/CD8+ ratio and increased production of proteases such as elastases, matrix metalloproteinases, and plasmin and elevated release of proinflammatory cytokines.[9−11] In this regard, macrophage reprogramming and tailoring of the immune system have grabbed much attention.[12]

In recent years, regenerative medicine has presented novel hi-tech dressing designs, which have achieved Food and Drug Administration (FDA) approval and are now commercially available.[13−16] Controlled delivery of bioactive molecules (e.g., cytokines, chemokines, and growth factors that are involved in wound-healing pathways) has been used in skin tissue engineering.[17−19] Also, cell-based therapies as another effective therapy have gained much attention. Cell therapy improves wound healing without major surgical processes and donor-site morbidity. Cell therapy can be used for acute and chronic wounds. In the therapy of acute wounds, cell therapy enhances the healing rate, decreases scar contracture, and reduces donor-site morbidity. This method also provides a tissue like the surrounding skin with minimal scars and color mismatch. Hence, cell therapy can solve the skin-grafting disadvantages including poor color matching in the recipient site and donor-site morbidity, including pain, discomfort, and hypertrophic scarring.[20] The main concerns of cell therapy are limited replicative lifespan, risk of teratoma formation after transplantation, and ethical issues.[21] Eukaryotic cells can be considered as robust natural bioreactors that produce a variety of bioactive molecules with the appropriate ratio, which can act as therapeutic agents in the wound-healing process and enhance the regeneration rate of the lost/damaged tissue.[22−24] Furthermore, recent investigations have revealed that multipotent, plastic mesenchymal stem cells (MSCs), which benefit from paracrine signaling, are highly potent to be utilized as allogenic sources for enhancing wound healing.[25,26] Paracrine signaling contributes to the regenerative ability of MSCs either through the whole secretome or even through the exosomes; this signaling has been reported to be effective in wound healing and scar reduction through modulating the ratios of MMP-3/TIMP1, TGF-β3/TGF-β1, and (type III collagen)/(type I collagen), which reduce the myofibroblast differentiation and eventually promote ECM reconstruction and wound healing.[27] As natural bioreactors, MSCs secrete lots of bioactive molecules, which could accelerate wound healing by increasing the migration of the dermal fibroblast and keratinocyte into the wound area, resulting in accelerated wound healing.[28,29] MSCs also increase the level of angiogenesis via increasing the levels of VEFG and HGF, increasing the microvessel density, and improving the microcirculation in the wound.[30,31] The immunomodulatory features of the MSCs can be harnessed to modulate the immune responses and inflammation.[32] MSCs also improve ECM remodeling via reducing matrix metalloproteinase (MMP-1) while increasing elastin and collagen.[4,33,34] In addition, MSCs affect skin regeneration via augmenting the thickness of the epidermis and skin appendages.[35]

There are different approaches for priming MSCs to augment their therapeutic properties such as adding proinflammatory cytokines to the culture medium, hypoxia conditions, and biomaterials. One of the most efficient ways to facilitate the priming of MSCs without incorporating chemical or exogenous conditions is utilizing the hanging-drop or spheroid culture system, which closely mimics the natural microenvironment and physiological condition of native tissues.[36−38] In addition, spheroid MSCs (S-MSCs) are more resistant under hypoxic conditions (i.e., in hypoxic wound milieu) in comparison to two-dimensional (2D) monolayer MSCs because in spheroid MSCs, the upregulation of hypoxia inducible factor I occurs and superoxide dismutase expression has been managed.[31,39] Three-dimensional (3D) S-MSCs also improve the angiogenic, anti-inflammatory, and immunomodulatory stemness and survival characteristics of the MSCs. Accordingly, S-MSCs have been proved to provide more therapeutic efficacy in healing wounds, compared to 2D monolayer MSCs.[31] However, cell viability and localization can be improved through the utilization of appropriate biomaterials. Moreover, these cell/biomaterial systems can serve as wound-dressing and delivery platforms for secretome.[40]

Conventional scaffolds and hydrogels act as passive dressing onto which cells can reside, proliferate, and migrate. This provisional extracellular matrix (ECM) maintains moist environments and may absorb exudates and kill pathogens. However, novel wound-healing and skin-regeneration strategies can help develop bioactive scaffold platforms that not only have cell-adhesive sites but also are rich in instructive cues.[41,42] Sodium alginate (SA) is a widely used polysaccharide with interesting properties such as high hydrophilicity, low toxicity, biodegradability, biocompatibility, nonantigenicity, unique ability to chelate with multivalent cations, tunable mechanical properties, and recapitulating key features of the ECM.[43−45] Moreover, alginate encapsulation could enhance the preservation period of MSCs, which is stored at 15 °C, while retaining their normal functions.[46] It can also provide opportunities for cell cryopreservation for future applications[47] Alginate encapsulation maintains the viability of S-MSCs and preserves the integrity of S-MSCs (i.e., impedes cell migration from spheroid aggregates). Moreover, they act as drug delivery platforms, which release the secreted bioactive molecules in a controlled manner while protecting them from the host's immune system responses (which is a major challenge) and mechanical stresses.[48,49] Encapsulated S-MSCs were further dispersed into a thermosensitive injectable hydrogel based on poly(*n*-isopropyl acrylamide) (PNIPAm) and gelatin. Thermosensitive polymers, due to their nature, show injectability performance, which solidifies contact with the body.[50−52] PNIPAm has a low critical solution temperature (LCST) of around 32 °C and rapidly undergoes sol-to-gel transition when absorbing heat from the skin.[53] Besides, PNIPAm-based hydrogels shrink at T > LCST because of water loss, which is highly interesting to make mechanically active adhesive dressings.[54] On the other hand, gelatin enhances the biocompatibility and biodegradability of the hydrogel and enhances the water retention properties of the composite hydrogel by absorbing the released water molecules from the PNIPAm structure.[55] This cross-linker-free injectable hydrogel could fill the space in deep wounds or in a defect with an irregular shape and also could cause wound contraction that consequently decreases the load and accelerates wound closure.[54] In addition, during motion, the risk of dislocation will be reduced by providing force transmission by close contact with adjacent tissues.[37,56]

IL-10 and TGF-β have been known as anti-inflammatory and immunomodulatory cytokines, which are found in MSC

https://dx.doi.org/10.1021/acsbiomaterials.0c00988
ACS Biomater. Sci. Eng. XXXX, XXX, XXX−XXX

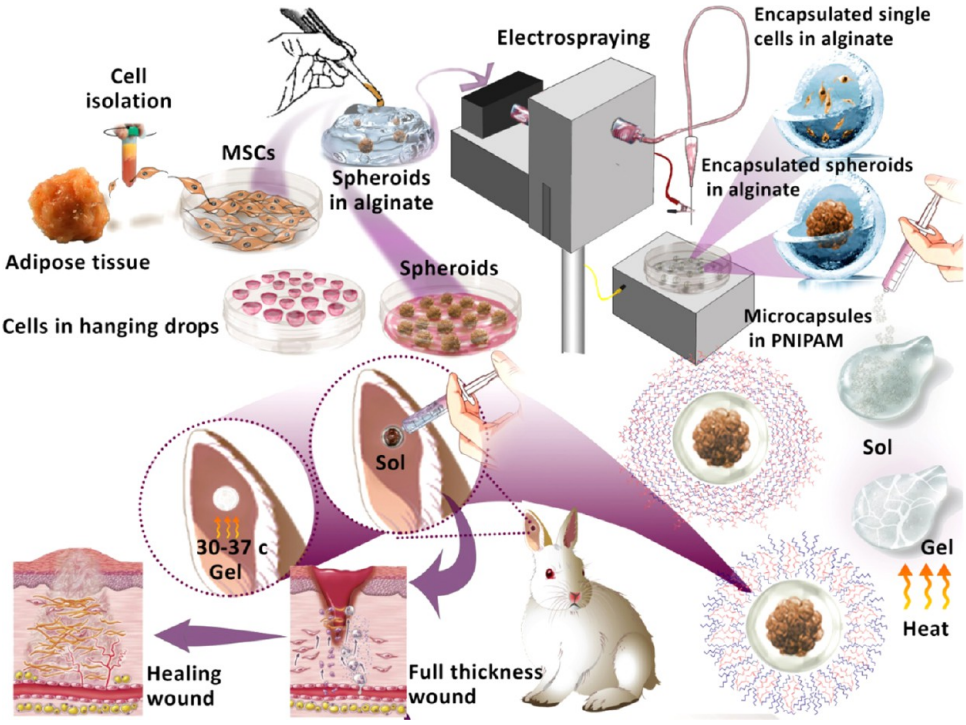

Figure 1. Schematic illustration of the electrospray setup used for microencapsulation.

secretomes. Immunomodulation is one of the most essential characteristics required for wound healing. Among MSC-derived immunosuppressive factors, IL-10 and TGF-β were noticed in the highest concentrations in MSC secretomes. Both IL-10 and TGF-β1 are involved in polarization of monocytes and M1 proinflammatory macrophages to the M2 anti-inflammatory macrophage phenotype. IL-10 has novel functions as a regulator of the extracellular matrix, fibroblast cellular function, and endothelial progenitor cells. TGF-β1-3 from the TGF-β superfamily plays critical roles in different phases of wound healing, and it is involved in almost every stage of wound healing. Among them, TGF-β1 is considered to be one of the main promoting factors for wound healing because the release of TGF-β1 at an early stage of wound healing prompts recruitment of inflammatory cells into the injury site, improves the angiogenic properties of endothelial progenitor cells to facilitate blood supply to the injured site, stimulates contraction of fibroblasts to enable wound closure, promotes keratinocyte migration by regulating cell-migration-associated integrins, and also it is a main collagen-stimulating factor and also inhibitor of different MMPs. Considering these extensive anti-inflammatory roles in wound healing, the evaluation of IL-10 and TGF-β1 concentrations seems to be necessary.[57,58]

In this study, an electrospray (ES) encapsulation apparatus was used to encapsulate individual or 3D spheroid MSCs into microscale alginate beads (microbeads). Due to the high concentration in the MSC secretome, pleiotropic effects, and being involved in all phases of wound healing, the levels of IL-10 and TGF-β1 have been investigated.[59−61] Furthermore, alginate microbeads were embedded in an injectable thermosensitive hydrogel matrix, which gels at skin temperature to fill and seal the wound cavities and maintain the humidity at the wound area as a strategy toward healing the chronic wounds.

2. MATERIAL AND METHODS

2.1. Cell Culture Procedure. Adipose-tissue-derived mesenchymal stem cells (ASCs) were isolated using the enzymatic method. Human adipose tissue samples were obtained from healthy females (18−30 years old) who underwent conventional liposuction of the abdomen, with informed consent signed by patients before liposuction. The adipose tissue was washed several times with sterile phosphate-buffered saline (PBS) and penicillin/streptomycin (5% w/w) to remove blood. Next, the samples were digested with collagenase type I (0.1%, Gibco) at 37 °C for 45 min. The digested fat was centrifuged at 1200 rpm for 10 min. The cell pellet, known as stromal vascular fraction (SVF), was resuspended in L-DMEM (BioIdea) containing 10% fetal bovine serum (FBS) (Gibco) and incubated in standard culture conditions (21% O_2, 5% CO_2, 37 °C) for 24 h. After that, nonadherent cells in suspension were removed, while MSCs adhered to the culture flask. Cells were characterized for expression of their typical lineage-specific CD markers by flow cytometry and examined for multiple lineage differentiation.

2.2. Spheroid Formation. ASCs from passages 3 to 5 were used to make spheroids. MSC spheroids were formed by applying the hanging-drop technique. In a typical procedure, 25 μL drops, each containing approximately 8000−10 000 cells, were placed on the inside of a Petri dish lid and quickly inverted on a plate containing 10 mL of PBS to prevent drying. After 24 h, gravity induces cell assembly in the hanging droplets, resulting in spherical aggregates; the aggregates were transferred to a nontissue-culture-treated six-well plate (Biofil). Then, spheroids were collected to be entrapped in alginate beads.

2.3. Cell/Spheroid Microencapsulation. Microencapsulation of individual MSCs and spheroids within alginate was performed separately in an electrospray setup, as schematically illustrated in Figure 1[62] Before electrospray, the required solutions were prepared. Alginate (alginic acid sodium salt, medium viscosity, purchased from Sigma-Aldrich: A2033-250G) was dissolved in warm Dulbecco's modified Eagle's medium (DMEM) under vigorous mixing to prepare 2% (w/v) alginate solution, followed by sterile filtration. This concentration was selected for microbead creation because for lower concentrations, the created microbeads were deformed or loose, while at higher concentrations, the viscosity of the solution was too high to

https://dx.doi.org/10.1021/acsbiomaterials.0c00988
ACS Biomater. Sci. Eng. XXXX, XXX, XXX−XXX

be sterile filtered, easily. Dissociated MSCs were resuspended in 2% alginate (medium viscous, Sigma-Aldrich) to yield a final solution of 2×10^6 cells/mL. On the other hand, approximately 200 spheroids were suspended in 1 mL of 2% alginate. The cell-alginate dispersion was transferred to a 2 mL syringe with a blunt needle 23G. Alginate solution should be extruded into an aqueous $CaCl_2$ solution (100 mmol/L) to create alginate beads. The Ca^{2+} cations in the solution ionically cross-link alginate chains to create alginate beads.

According to Figure 1, the electrospray setup was sterilized using ethanol and UV irradiation for 0.5 h, before the encapsulation process. The syringe was filled with an alginate/DMEM solution containing either cells or spheroids, under sterile conditions. A Petri dish containing a sterile aqueous $CaCl_2$ solution was placed beneath the syringe such that the needle tip distance from the $CaCl_2$ solution was fixed at 10 cm. The flow rate of the alginate solution was controlled by a micropump; besides, the needle tip and the metal plate over which the $CaCl_2$ solution is placed were connected to a high-voltage power supply. The applied potential difference between these electrodes polarizes the solution, exerting a tensile force such that small droplets with tunable sizes can be created. Submerged alginate droplets were ionically cross-linked by Ca^{2+} cations, making alginate microbeads. To induce cross-linking, microbeads were incubated in the $CaCl_2$ solution for 10 min at room temperature before they were washed with sterile distilled water, three times. It was observed that application of a voltage of 10 kV and a setting flow rate at 7 mL/h result in alginate microbeads of the desired diameter (approximate diameter: 200−300 μm) that can effectively encapsulate S-MSCs.

2.4. Cell Viability Assessment. After 7 days of culturing, the viabilities of free S-MSC, S-MSCs@MB, and MSC@MB were analyzed by double fluorescent staining using a LIVE/DEAD cell assay reagent (Abcam). Gels were thoroughly immersed in 5× solution of calcein AM and EthD-1 followed by incubation for 30 min at room temperature; the obtained product was completely washed using PBS, and a fluorescence microscope was used to take photographs.

Cell viability was measured quantitatively by flow cytometric analysis (on ca. 2×10^4 cells) using Annexin V FITC/propidium iodide staining solution, after 7 and 12 days of culturing. To release the cells from alginate microbeads, the microbeads were immersed in 100 mM trisodium citrate (Sigma-Aldrich) for 10 min followed by diluting with PBS. The obtained suspension was centrifuged at 1200 rpm for 5 min after which the supernatant was removed. Then, cells/spheroids were treated with trypsin to obtain individual cells.

2.5. Thermosensitive Hydrogel Formulation. PNIPAm is a thermosensitive polymer whose LCST is around 32 °C. To enhance water retention beyond LCST, gelatin was blended with PNIPAm to make a semi-interpenetrating polymer network (semi-IPN); moreover, gelatin improves biodegradation and biocompatibility of the resulting hydrogels. In a typical procedure, a 2 wt % gelatin aqueous solution was prepared by dissolving 0.1 g of gelatin in 5 mL of distilled water while stirring. The solution temperature was increased slightly to enhance the dissolution rate. After complete dissolution of gelatin, 0.25 g of NIPAM and 6 mg of APS were added to the solution and stirred for 0.5 h to assure complete dissolution. Finally, 20 μL of tetramethylethylenediamine (TEMED) was added to the solution while stirring under a nitrogen (N_2) atmosphere. The reaction proceeded while stirring for 2 h at room temperature followed by 0.5 h of stirring at 70 °C to assure complete reaction. All of the materials in this procedure were purchased from Merck.

2.6. Rheological Evaluations. Rheological measurements for aqueous solutions were performed using an Anton Paar-Physica MCR 300 rheometer (Anton Paar, GmbH, Germany). Temperature sweep experiments (angular frequency: 1 rad/s; strain: 1%; heating rate: 1 °C/min) were conducted in the temperature range of 5−45 °C to study the sol−gel transition behavior of the hydrogels.

2.7. Cytokine Secretion. Cell/microbeads (MSC@MB) or spheroid/microbeads (S-MSC@MB) were suspended in a complete medium and incubated under standard culture conditions. Under these conditions, the MSCs continually produce secretomes, which gradually diffuse through the porous structure of alginate microbeads, which act as a hydrogel membrane.[63] The concentration of secreted macromolecules in the surrounding complete medium is zero at the beginning but increases gradually. Besides, the mass transfer rates of various biological macromolecules through the porous structure of alginate microbeads (see Figure 5) are different. The overall function of S-MSCs is higher than individual MSCs, resulting in different concentrations of secreted macromolecules in MSC@MB and S-MSC@MB systems, which should be evaluated, experimentally.

In this regard, an experimental procedure was performed to evaluate the concentrations of IL-10 and TGFβ-1 cytokines in the complete medium. Evaluation of cytokine secretion was performed on days 1, 3, and 5 after incubation. In a typical experiment, after centrifuging the microbead suspension, 1 mL of supernatant (1 mL) was removed and stored at −70 °C for further measurements of cytokine concentration. Then, 1 mL of a fresh complete medium was added to the microbead suspension before replacing in the incubator. The concentrations of secreted cytokines (IL-10 and TGFβ-1) in the supernatants (or conditioned medium (CM)) were measured by sandwich ELISA kits (Peprotech and Biolegend) according to the manufacturer's instructions. The experiments were repeated in triplicate (n = 3) and normalized to DMEM + FBS 10%. It is worth mentioning that each well contained a total of 1.6×10^5 cells in either the monolayer or spheroid culture, with spheroids in alginate microbeads.

2.8. Rabbit Ear Full-Thickness Model. This study was approved by the Ethics Committee of the Tehran University of Medical Sciences (ethical code; IR.TUMS.VCR.REC.1397.257). The rabbit ear full-thickness model has been well established. Briefly, 12 adult albino rabbits (each weighing 4−5 kg) were anesthetized using ketamine/xylazine under sterile conditions. Three circular, full-thickness, 8 mm wounds were punched to the cartilage on the surface of both ears and randomized by location. The rabbits were divided into four treatment groups as represented in Table 1.

Table 1. Different Treatment Groups of Rabbits

sample	composition	notation
(A)	nothing applied	untreated
(B)	pristine sodium alginate microbeads/ hydrogel	MB/hydrogel
(C)	MSCs in sodium alginate microbeads in hydrogel	MSC@MB/ hydrogel
(D)	spheroids in sodium alginate microbeads in hydrogel	S-MSC@MB/ hydrogel

Each wound was filled with approximately 0.2 mL of hydrogel containing 30 microbeads (i.e., containing MB or MSC@MB or S-MSC@MB) followed by covering by occlusive dressing. After that, the rabbits were individually housed and fed. On days 7 and 14 after the first treatment, wounds were replenished with excessive hydrogel of the same composition. Wound healing was assessed on days 0, 7, 14, and 21 after treatment.

2.9. Histological Analysis. Rabbits were sacrificed on days 7, 14, and 21 after treatment, and their ears were cut off for further histological examinations. On each ear, three wound areas were excised and fixed in 10% formalin. After tissue processing, they were embedded in paraffin wax and cut into 7 μm thick sections. After deparaffinization and rehydration, the prepared specimens were placed on slides and were stained with hematoxylin and eosin (H&E). Moreover, Masson's trichrome staining was used to evaluate the collagen level and its arrangement pattern in the wound area. Images were taken using an Olympus inverted microscope and a digital camera.

Immunohistochemistry (IHC) analysis was carried out by α-smooth muscle actin (α-SMA) (1:100, Abbexa) and CD31 (1:100, Bioss) antibodies conjugated to the peroxidase enzyme. The presence of proteins was detected using DAB as the substrate of the enzyme.

2.10. Statistical Analysis. ImageJ software was used to quantitatively analyze the epithelial thickness and the average optical density values for collagen, α-SMA, and CD31 histochemical

https://dx.doi.org/10.1021/acsbiomaterials.0c00988
ACS Biomater. Sci. Eng. XXXX, XXX, XXX−XXX

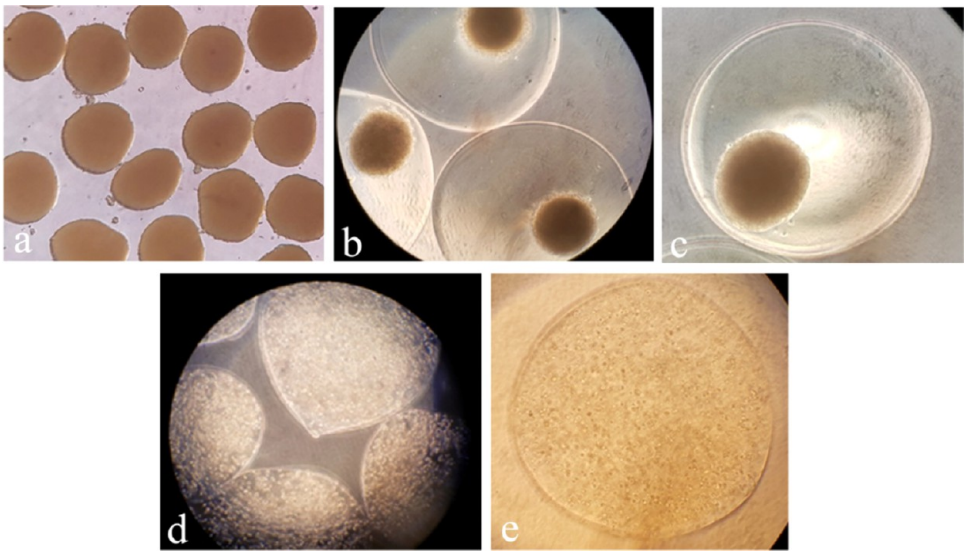

Figure 2. Digital photographs of S-MSCs and encapsulation of S-MSCs and MSCs applying the electrospray setup. (a) Spheroid formation of MSC using the hanging-drop technique (almost 8000 cells per 25 μL drop), 10× magnification. (b, c) Entrapped spheroids in alginate microbeads with sizes (200−300 μm) 10× and 20× magnification, respectively. (d, e) MSCs encapsulated in alginate microbeads with sizes (200−300 μm) 10× and 20× magnification, respectively.

assessments. The average optical density value was calculated per millimeter of area. At least three independent experiments were performed for each assay, and data are reported as mean ± standard error of the mean (SEM). Two-way analysis of variance (ANOVA) followed by Tukey's post-test Graph Pad prism 4.02 software was used to compare multiple conditions. Values of $p \leq 0.05$ were considered statistically significant.

3. RESULTS

3.1. Optimization of S-MSC Formation. To make spheroids with proper shape and biological activity, we optimized the number of MSCs for spheroid formation in the hanging-drop method. It was observed that spheroids with low cell densities (less than 1000 in each 25 μL drop) did not aggregate properly within 24 h; they required longer times (48−72 h) to aggregate, which may result in insufficient nutrient supply. On the other hand, high cell densities (i.e., more than 10 000 cells per drop) resulted in the formation of a loose network containing several small nonuniform aggregates. It is revealed that there is an optimum cell density (approximately 8000 cells per 25 μL drop) that can generate densely packed spheroids, after 24 h. There were no observable dark apoptic cores in the obtained spheroids that could be created as a result of hypoxia, low nutrients, and waste accumulation (see Figure 2a).

3.2. MSC/S-MSC Microencapsulation. Alginate encapsulation is an effective solution to prevent spheroid agglomeration and to maintain their integrity and viability.[64] Electrospraying was utilized to entrap individual cells or spheroids in alginate microbeads with tunable sizes (200−300 μm). Different parameters such as alginate concentration (1−2.5%, w/v), flow rate of alginate solution (5−10 mL/h), applied voltage (5−10 kV), concentration of cross-linking ions (50−150 mM Ca^{2+}), and spraying distance (5−15 cm) were considered. For alginate solutions containing less than 2 wt %, cells are unevenly distributed, tending to gather on one side of the gel. Aqueous solutions containing calcium chloride are detrimental to the cells (especially when the concentration is higher than 1.5 wt %) such that $CaCl_2$ concentration and immersion time of microbeads should be minimized.[65] It was found that 100 mM $CaCl_2$ is the minimum concentration for which the alginate solution is rapidly cross-linked, leaving minimal encapsulated cells.

The applied voltage was altered when fixing the distance between the needle tip and the cross-linking solution to 10 cm. It was observed that for applied voltages less than 9 kV, the bead diameter is larger than 1 mm. On the other hand, as applied voltages increase beyond 10 kV, the bead diameter reduces to less than 100 μm. In the optimal range of 9−10 kV, the diameter of the final cross-linked microbeads was approximately 200−300 μm. It is possible to encapsulate MSCs or S-MSCs within these microbeads, as shown in Figure 2. Microbeads with less diameter values may fail to completely encapsulate S-MSCs, while higher diameter values limit the application of microbeads on the wound.

3.3. Cell Viability in Microbeads. The viability of encapsulated MSCs (i.e., MSC@MB) was qualitatively analyzed, using fluorescent staining by Calcein AM/EthD, after 7 days of incubation in a standard culture condition. A few visible red cells, which indicate dead cells, were observed in S-MSC@MB (Figure 3b), while more red cells were observable in MSC@MB (Figure 3d). However, cellular apoptosis/necrosis was quantitatively studied using Annexin V/Propidium iodide (PI) staining in flow cytometry measurements. As illustrated in Figure 4a, after 7 days, 83.1% of the cells were viable in S-MSCs, while 14.0% were necrotic. The necrotic cells are more likely located in the spheroid core where there are hypoxia and nutrient deficiencies. Cell viability increased to 92.8% after 12 days (Figure 4b), which can be interpreted as hypoxia-induced adaptations of S-MSCs in microbeads, similar to tumor spheroids.[66] Moreover, spheroid growth was also observed in alginate microbeads. For individual MSCs (i.e., MSC@MB), more dead cells were observed and cell viability was measured to be 81.4% (Figure 4c). MSC viability decreased to 78.3% on day 12 (Figure 4d). Increasing cell viability in S-MSCs and the slight reduction in MSC viability indicate that alginate provides a good microenvironment for maintaining cell and spheroid survival at least

https://dx.doi.org/10.1021/acsbiomaterials.0c00988
ACS Biomater. Sci. Eng. XXXX, XXX, XXX−XXX

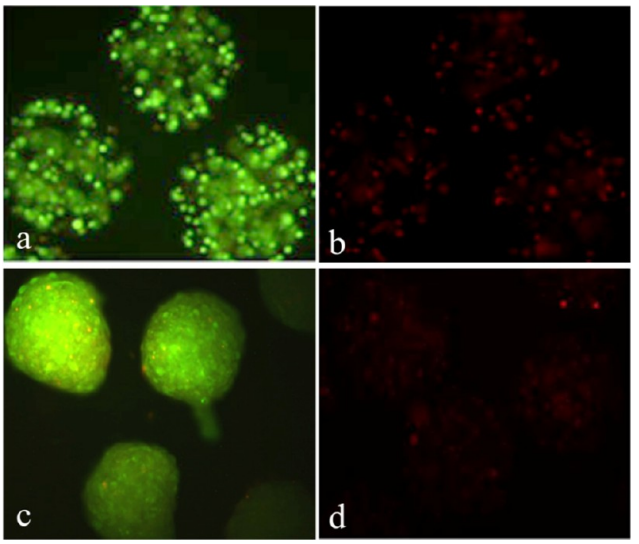

Figure 3. Calcein AM/EthD viability assay for encapsulated MSC and S-MSC. (a) Green fluorescence of live cells in alginate-encapsulated MSCs (MSCs@MB) using a band pass filter of 470−490 nm after 7 days. (b) Red fluorescence, which demonstrates more dead cells in alginate-encapsulated MSCs (MSCs@MB) in comparison to S-MSC@MB using a band pass filter >520 nm after 7 days. (c) Green fluorescence of live cells in alginate-encapsulated S-MSCs (S-MSCs@MB) using a band pass filter of 470−490 nm after 7 days. (d) Red fluorescence, which demonstrates fewer dead cells in alginate-encapsulated S-MSCs (S-MSCs@MB) in comparison to MSC@MB using a band pass filter >520 nm. 20× magnification.

for 2 weeks. Furthermore, the effect of the electrospraying process on cell viability was negligible.

3.4. Microbead Microstructure. The topological features of microbeads were investigated by scanning electron microscopy (SEM, AIS2300C, Seron Technologies Inc., South Korea). After lyophilization, the microbeads were cryogenically fractured in liquid nitrogen, before gold sputtering. SEM images of cross sections of beads showed uniform interconnecting porous structures, as illustrated in Figure 5. The microbead diameter was around 200 μm

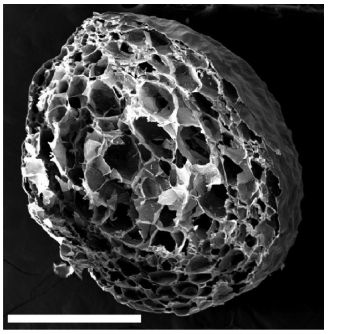

Figure 5. Scanning electron microscopy (SEM) images of microbeads. Uniform interconnecting porous structure of the alginate microbead. Scale bar is 100 μm.

although there is a pore-diameter distribution. This porous structure facilitates the convection and diffusion of mass transfer for various cytokines. An upper coating envelopes this

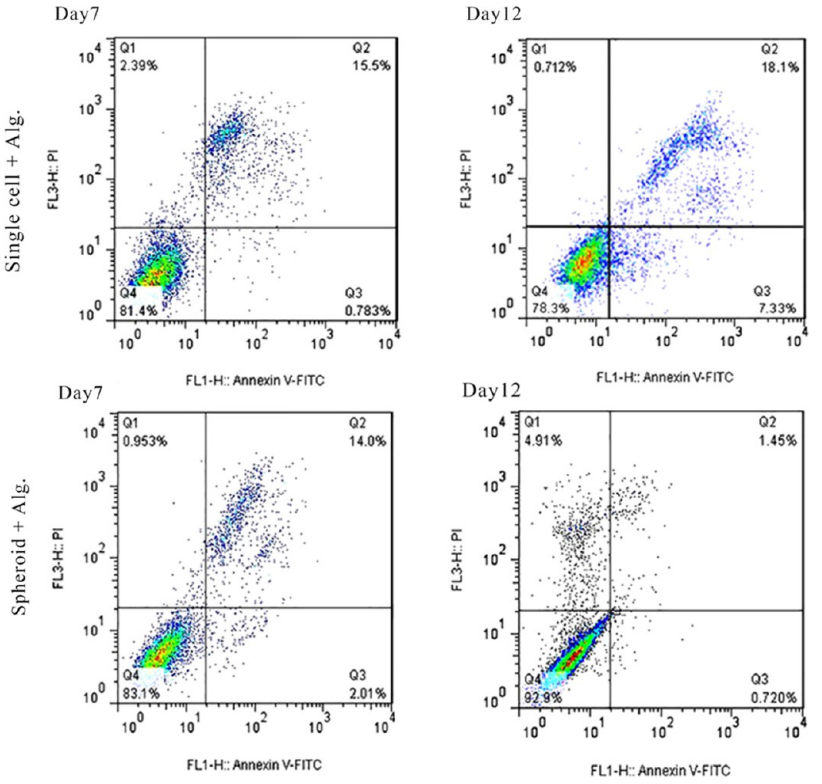

Figure 4. Flow cytometry analysis of cell viability using Annexin V (FL1-H) and PI (FL3-H) staining. (a) 81.4% of viable MSCs@MB after 7 days. (b) Decrease of viability of MSCs@MB from 81.4 to 78.3% after 12 days. (c) 83.4% of viable S-MSCs@MB and 14% necrotic S-MSCs@MB (due to locating at the core of the spheroid and affected by hypoxia and starvation conditions) after 7 days. (d) Increase of viability of S-MSCs@MB from 83.4 to 92.8% after 12 days.

https://dx.doi.org/10.1021/acsbiomaterials.0c00988
ACS Biomater. Sci. Eng. XXXX, XXX, XXX−XXX

porous structure, which is more likely a result of ion cross-linking of alginate in excess Ca^{2+} ions. This envelope prevents fast release of cytokines by convection mass transfer.

3.5. In Situ Gelation of Copolymer on Wounds. To investigate the sol−gel transition of the hydrogel on the skin/wound area, the rheological properties of the composite hydrogel were investigated using a rheometer in the temperature sweep mode. Moreover, the gelation time of the hydrogel was measured using the time sweep of the inversion method at 37 °C. The gelation time was around 3.7 min. Figure 6 shows

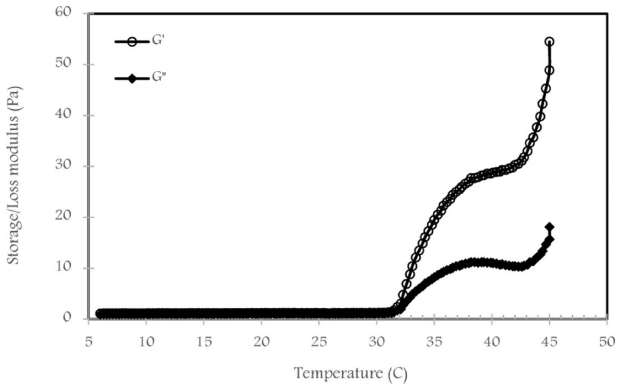

Figure 6. Rheological characterization of the injectable composite hydrogel for investigating sol−gel transition in the temperature sweep mode. Variations of G' and G'' as a function of temperature for the injectable composite hydrogel.

the variations of the storage (G') and the loss (G'') modulus of the hydrogels as a function of temperature. Neither the storage nor the loss modulus exhibits remarkable changes in the range of 5−31 °C. However, at sol−gel transition temperature (at around 32 °C), their values suddenly increase. As temperature increases beyond $T_{sol-gel}$, G' grows more rapidly compared to G''. A higher storage modulus at $T > T_{sol-gel}$ indicates more elastic behavior of the hydrogel. This behavior confirms the gelation of the composite hydrogel at temperature ranges close to the skin surface. In other words, this injectable hydrogel can be successfully used in wound-healing applications.

Approximately 0.2 mL of hydrogels was applied, for each wound, right after making circular incisions. When applying on the wound area, it was observed that the PNIPAm/gelatin hydrogel can effectively fill the wound gaps before experiencing sol−gel transition within minutes (see Figure 7). The thermosensitive hydrogel formed a semisolid white gel that surrounds the alginate microbeads minimizing the microbead movement. The hydrogel ensures efficient contact between the skin tissue and microbeads even in movements; moreover, it protects the secretome from the harsh wound microenvironment and direct contact with air, enhancing the stability of secreted proteins. Furthermore, it serves as a controlled drug delivery platform for microbeads, which are in situ drug synthesis platforms. The space-filling characteristic of the hydrogel in deep wounds brings about comfort and close contact of cells with lost tissue.

3.6. Cytokine Secretion. The secretion pattern of two important cytokines in the wound-healing process (IL-10 and TGF-β1) was assessed by enzyme-linked immunosorbent assay (ELISA). As shown in Figure 8, 3D culture of cells either in the

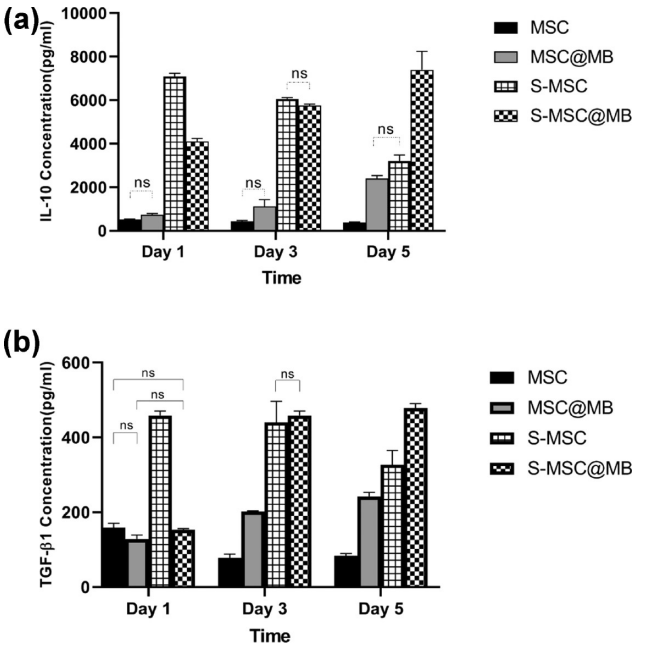

Figure 8. Concentrations of secreted cytokines, in picogram per milliliter (pg/mL), versus time for (a) IL-10 and (b) TGF-β1. There are significant differences between groups other than shown on the chart (ns). P-value < 0.05.

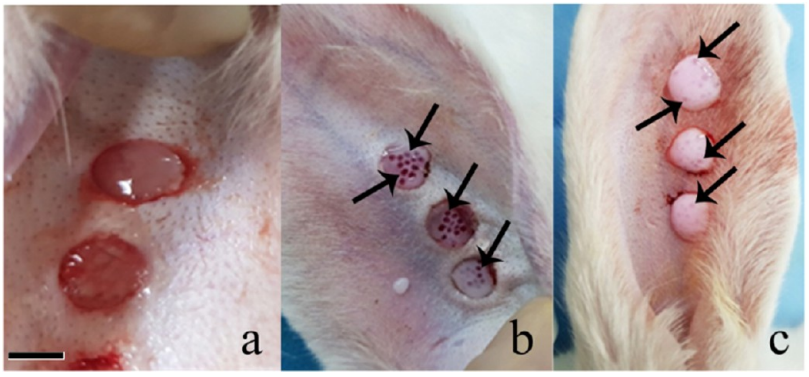

Figure 7. Application of dispersed MB, MSCs@MB, or S-MSCs@MB into the thermosensitive PNIPAm/gelatin hydrogel dressing on a full-thickness wound model on rabbit ear: (a) right after injection, which behaves like a transparent viscous fluid; and (b) after 3 min of injection, which shows sol-to-gel transition resulting in a translucent fluid. The arrows indicate the alginate microbeads in PNIPAm/gelatin (c) after 5 min of injection, which formed a semisolid white gel fixing alginate microbeads. Scale bar is 10 mm.

https://dx.doi.org/10.1021/acsbiomaterials.0c00988
ACS Biomater. Sci. Eng. XXXX, XXX, XXX−XXX

spheroid form (i.e., S-MSCs) or in alginate microbeads (i.e., MSC@MB) significantly promotes the secretion of IL-10 and TGF-β1. The concentration of IL-10 is generally higher than that of TGF-β1. On the first day after encapsulation, the concentration of both cytokines secreted by spheroids was the highest among all groups. The concentration of IL-10 is more than seven times higher for S-MSCs compared to MSCs or MSC@MB, while this ratio is less than 3 for TGF-β1, indicating that 3D culture has a more profound impact on the secretion of IL-10 compared to TGF-β1. On the other hand, the concentration of IL-10 for encapsulated spheroids (S-MSC@MB) relative to free spheroids (S-MSCs) is around 50%, while for TGF-β1, this ratio is much less; this indicates a lower mass transfer for TGF-β1 compared to IL-10. Encapsulation in alginate results in a more gradual/controlled release of cytokines similar to controlled drug release systems. However, there are no significant differences between secreted cytokines from free and encapsulated MSCs on the first day.

On day 3, there were only slight differences between free spheroids and encapsulated spheroids in terms of secreted factors. On the other hand, the difference between concentrations of secreted cytokines was enhanced for MSC and MSC-MB; i.e., secretion of both cytokines was higher for encapsulated cells, indicating that alginate encapsulation extends the cell activity. This behavior is also observed for spheroids, as well.

The most significant differences between different groups were observed on day 5. Cytokine secretion from free S-MSCs diminished, while the opposite trend could be observed for S-MSC@MB; a similar trend was observed for individual MSCs. In other words, alginate encapsulation enhanced the cytokine secretion from both MSCs and S-MSCs. In contrast, cytokine secretion from free MSCs or free S-MSCs decreased over time. This behavior can be interpreted as a gradual decrease in cell viability/activity for free MSCs or S-MSCs.

3.7. Wound Contraction Acceleration Using S-MSC@MB. The gross observation of the wounds 7 days post treatment revealed much faster contraction of the wounds in the S-MSC@MB-/hydrogel-treated group compared with other groups, as shown in Figure 9. On day 14, there was no obvious symptom of the unhealed wound area in the S-MSC@MB-/hydrogel-treated group in which the residual wound area was 4.5 ± 4; in contrast, the residual wound areas were 19.25 ± 4.57, 40.5 ± 5.325, and 47.81 ± 0.66% for the MSC@MBs/hydrogel, MB/hydrogel, and control (untreated) groups, respectively. On day 21, the remaining wound area in the MSC@MB-/hydrogel-treated group was negligible, but the polymer could not re-epithelialize the wound completely and 20.25 ± 2% of the wound area remained in the MB-/hydrogel-treated group. Residual wound area for different groups is depicted in Figures 10 and 11.

3.8. Histological Assessments. Histomorphological study of wound regeneration in different phases was performed by H&E and Masson's trichrome staining. Histological observations in all different groups revealed that the infiltration of lymphocytes, which is illustrated with dark nuclei and negligible cytoplasm, increased in the early days after wound creation, for all groups. However, these cells were found in the area around the arteries and in the connective tissue below the epithelium, even 14 days post wounding in the negative control and the MB/hydrogel-treated groups. The lymphocyte population was observed to diminish in the groups that were treated by the S-MSC@MB/hydrogel and the MSC@MB/

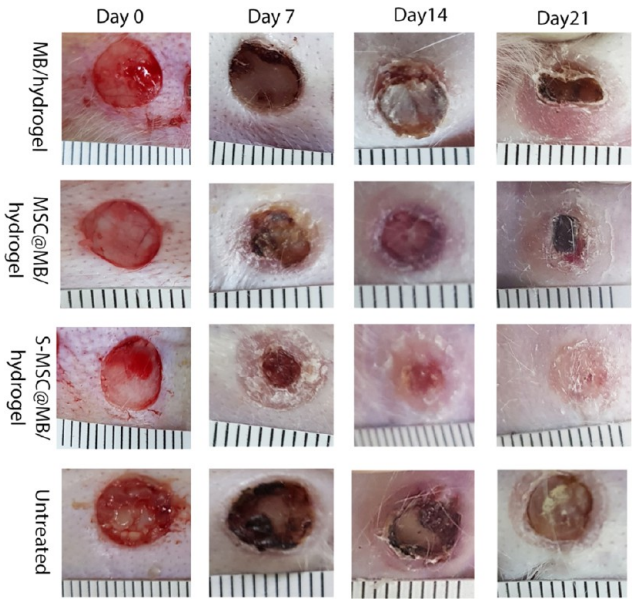

Figure 9. Digital photographs of wound-healing progression in untreated, MB/hydrogel, MSC@MB/hydrogel, and S-MSC@MB groups on days 0, 7, 14, and 21 post wounding. The contraction of the wound in S-MSC@MB was faster (day 7) than the other groups. Also, no visible scars can be seen in this group on day 21. The punches are 8 mm in diameter.

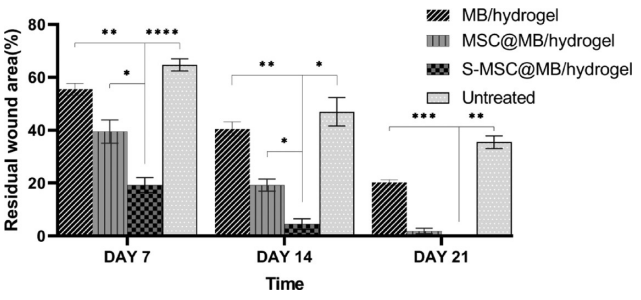

Figure 10. Percentage of residual wound in MB/hydrogel, MSC@MB/hydrogel, S-MSC@MB/hydrogel and untreated groups on days 0, 7, 14, and 21. There is a significant reduction in wound size between S-MSC@MB/hydrogel and other groups through healing time except for the MSC@MB/hydrogel and the S-MSC@MB/hydrogel on day 21. All image analyses have been performed using ImageJ software, and the resulted data have been calculated by two-way ANOVA and GraphPad Prism 4.02 software.

hydrogel on day 21 compared to day 7, indicating the gradual attenuation of inflammation. In all groups, the epithelial layer formed over time, although the population and layer of epithelial cells varied in different groups and on different days. In other words, on day 21, in the groups treated with S-MSC@MB/hydrogel and MSC@MB/hydrogel, this layer was reconstructed uniformly. However, in the negative control group, there was a thin epithelial layer full of vacuoles and a scarring layer on it. As shown in Figure 12, the epithelium thickness is increased with an accelerated slope in the untreated and MB/hydrogel groups, which may be due to scar formation and epithelium hyperplasia. Skin appendages, including hair, sebaceous glands, and sweat glands, were not observed in any of the groups and at any time; however, the depressions or accumulations indicated the leakage of epithelial cells inward to create the first layers of hair follicles

https://dx.doi.org/10.1021/acsbiomaterials.0c00988
ACS Biomater. Sci. Eng. XXXX, XXX, XXX−XXX

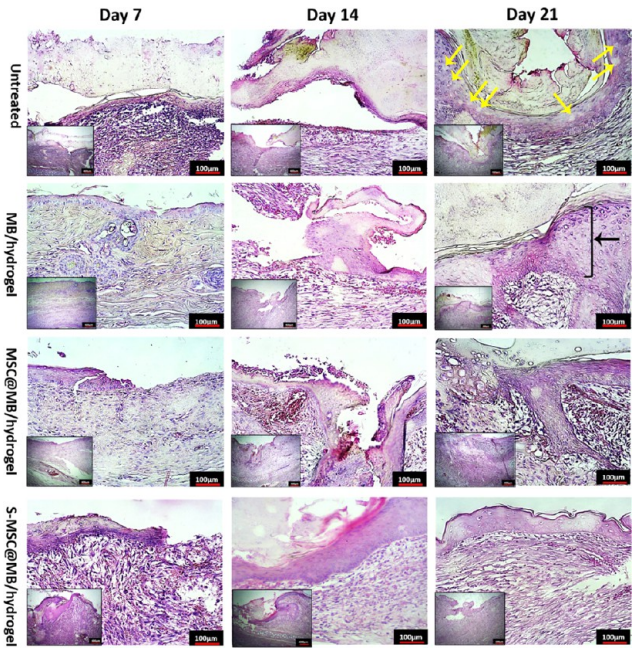

Figure 11. HE staining of the wound on days 7, 14, and 21 after treatment in MB/hydrogel, MSC@MB/hydrogel, S-MSC@MB/hydrogel, and untreated groups. Note that by day 14 complete re-epithelialization and granulation tissue was apparent in the S-MSC@MB/hydrogel group. Vacuoles (yellow arrows) can be seen in the epidermis on day 21 in the untreated group. In the MB/hydrogel group, a very thick layer of epithelium (black arrow) indicates scar formation. Scale bars are 400 μm (low magnification) and 100 μm (high magnification).

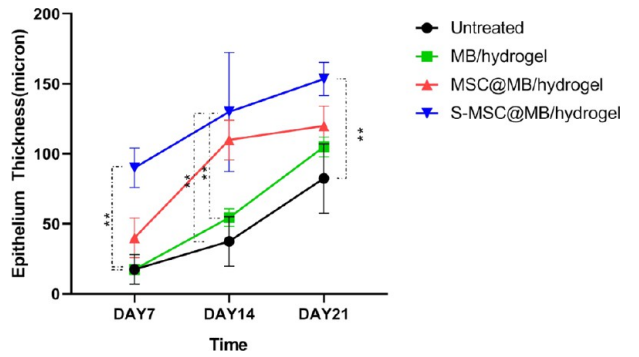

Figure 12. Epithelium thickness measurements in all groups through 21 days of wound healing. On day 7, there are significant differences of epithelium thickness between MSC@MB and S-MSC@MB groups versus each of no treatment and MB/hydrogel groups; on day 14, there is no significant difference in epithelium thickness between MSC@MB and S-MSC@MB; and on day 21, there is an increase in epithelium thickness of all four groups but with a steep slope in no treatment and MB/hydrogel.

in the single MSC@MB-/hydrogel-treated group. In this regard, it is probably necessary to study the quality of wound healing for a longer period of time.

The spindle-shaped cells with elongated nuclei and dense cytoplasm are fibroblasts. They are present in all stages of the wound-healing process, in both the dermal and the epithelial basal layer. Since these cells are responsible for collagen production, the population of these cells gradually increased in all groups from 7 to 21 days, after healing started. The fibroblast population was the highest for the group treated by the MSC@MBs/hydrogel and the S-MSC@MB/hydrogel.

Masson's trichrome staining was performed to detect collagen fibers, as illustrated in Figure 13. In two groups

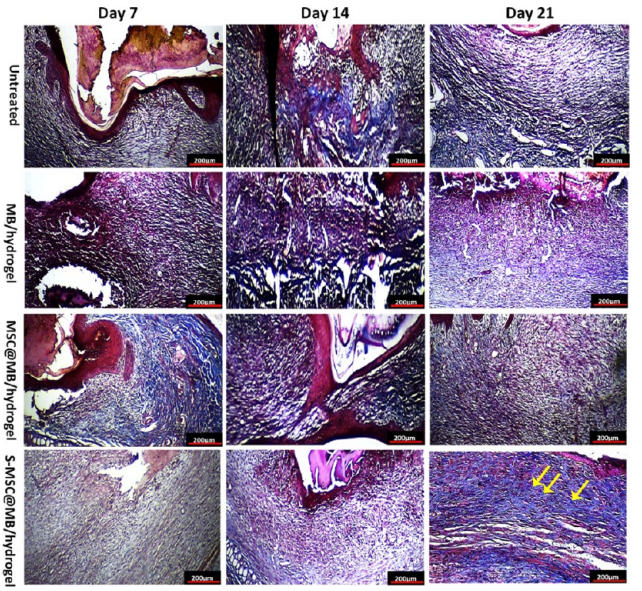

Figure 13. Histological assessment of collagen deposition by Masson's trichrome staining. Note that scattered collagen fibrils can be seen between all groups on days 7 and 14. The highest level of collagen density between all groups was for S-MSC@MB on day 21, and the pattern of its formation is regular and parallel to the epithelium (yellow arrows). Scale bar is 200 μm.

with more population of fibroblast cells, it was found that the amount of collagen clusters in the form of collagen type I and type III was more common. These dense clusters are well represented by the yellow arrows on day 21 for the S-MSC@MB-/hydrogel-treated group. It was observed that the intensity of blue collagen fibers regularly increased as confirmed by ImageJ and depicted in Figures 14−16.

In the S-MSC@MB-/hydrogel-treated group on day 21, normal orientations of collagen fibrils, which are parallel to the skin surface, were observed. In the untreated group and MB-/hydrogel-treated groups, the collagen filaments were often observed as a network; besides, more separated (individual)

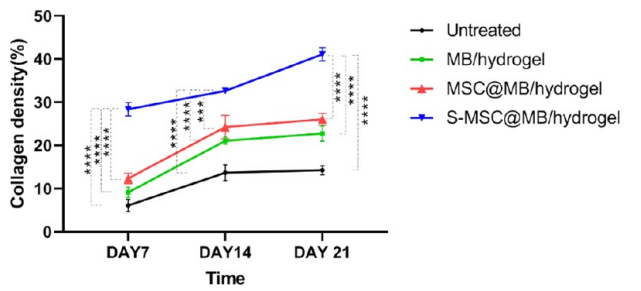

Figure 14. Collagen density measurement in untreated (control), MB/hydrogel, MSC@MB/hydrogel, and S-MSC@MB groups on days 7, 14, and 21. There is no significant difference between MB/hydrogel and MSC@MB groups on any day or time and significant difference in collagen density between S-MSC@MB and other groups on days 7, 14, and 21. ****$p < 0.0001$.

https://dx.doi.org/10.1021/acsbiomaterials.0c00988
ACS Biomater. Sci. Eng. XXXX, XXX, XXX−XXX

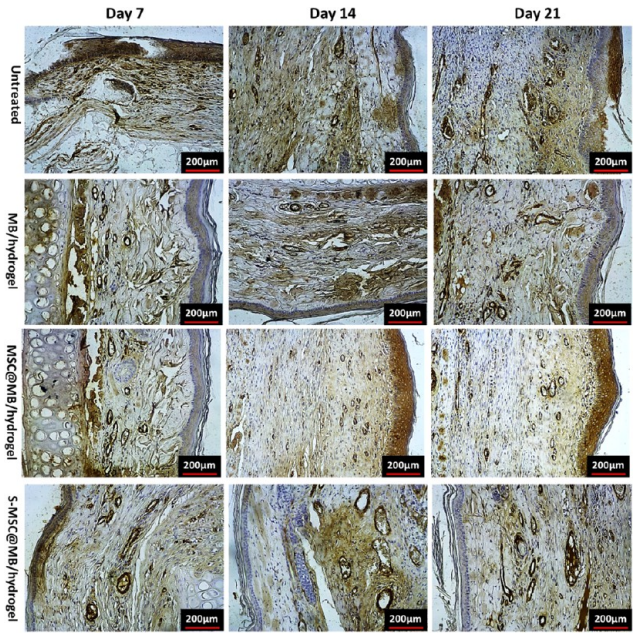

Figure 15. α-SMA immunohistochemical staining for detection of differentiated fibroblast to myofibroblast as an indicator of wound contraction and scar formation in untreated, MB/hydrogel, dispersed MSC@MB/hydrogel, and S-MSC@MB/hydrogel groups on days 7, 14, and 21 in wound sites. α-SMA is also expressed in smooth muscle cells of vessel walls. Scale bar is 200 μm.

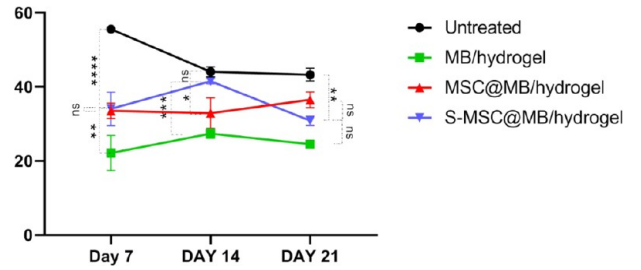

Figure 16. α-SMA percentages on days 7, 14, and 21 for different treatment groups. No treatment group has the highest level of α-SMA expression between all groups, and MB/hydrogel has the lowest expression; there is no significant difference in α-SMA expression between MSC@MB and S-MSC@MB groups on days 7 and 21, but the α-SMA expression was significantly ($*p < 0.05$) decreased on day 14.

filament strands were formed unlike the cohesive collagenic clusters, which are usually observed in normal tissues.

Mature fibroblasts, which express α-SMA, differentiate to myofibroblasts, which are responsible for wound contraction.[67] α-SMA is also expressed in the endothelial cells of blood vessels in the skin. Higher expression of this biomarker was observed in the untreated group compared to other groups, even until day 21, which is an indication of scar formation.[67] In the S-MSC@MB-/hydrogel-treated group, on day 14, the highest level of α-SMA through a 21 day wound-healing duration results in accelerated wound contrition. Further decrease of α-SMA in the following week improved the quality of wound healing. The overall higher level of α-SMA in this treatment group compared to the MB/hydrogel group may be related to more blood vessel formation and wound contraction. In the groups treated with MB/hydrogel and MSC@MB/hydrogel, moderate and constant expressions of α-SMA indicate gradual wound closure but with undesirable quality.

As demonstrated in Figures 17 and 18, applying cells in the spheroid form or single cells in the dressing enhanced

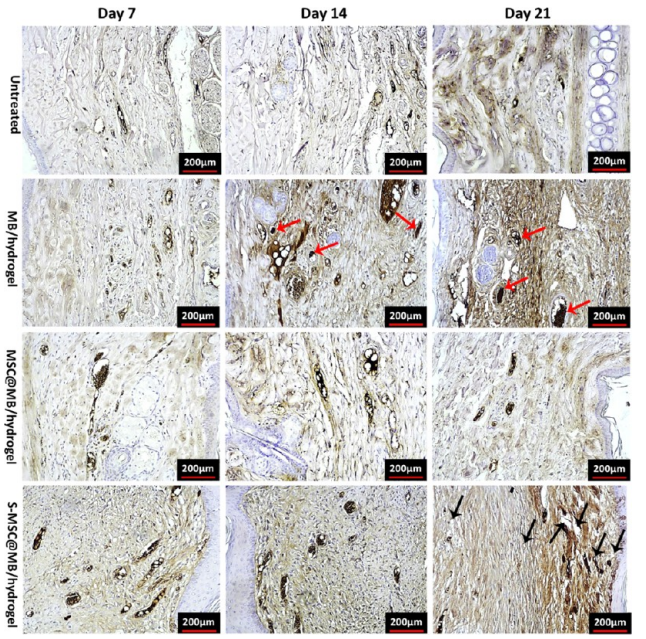

Figure 17. CD31 immunohistochemistry analysis of tissues from the wound site for demonstrating the presence of endothelial cells in different treated groups on days 7, 14, and 21. On days 14 and 21, the S-MSC@MB/hydrogel group presented with a highly microvascularized granulation tissue (red arrows); intensively stained thick veins may be due to the RBC endogenous peroxidase reaction with DAB in the MB/hydrogel (green arrows). Scale bar is 200 μm.

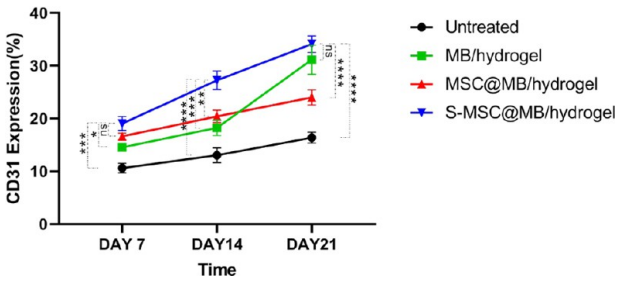

Figure 18. Percentage of the CD31 expression level as a marker of angiogenesis in wound healing in untreated (control), MB/hydrogel, MSC@MB/hydrogel, and S-MSC@MB groups on days 7, 14, and 21.

revascularization on day 7. However, at that time, there was no significant difference in the CD31 expression between these two groups. On day 14, vascularization between the MB/hydrogel and MSC@MB/hydrogel groups was not significant. On day 21, the CD31 expression percentage was similar in the MB/hydrogel and S-MSC@MB/hydrogel groups. However, thick and old veins can be recognized in the MB/hydrogel group that is filled with red blood cells. This may cause a miscalculation of color density in ImageJ software due to the RBC endogenous peroxidase reaction with DAB in the MB/hydrogel.

https://dx.doi.org/10.1021/acsbiomaterials.0c00988
ACS Biomater. Sci. Eng. XXXX, XXX, XXX−XXX

4. DISCUSSION

Current regenerative approaches in the treatment of long-lasting chronic wounds obviates the requirements for substituting the damaged tissue with skin allografts through transplantation of self-renewable stem cells; these stem-cell-based therapies have excessive expansion capacity.[22,25] The beneficial effects of MSCs are attributed to their secretome and paracrine communications with other neighboring cells. Clinical MSC-based therapies have shown effective outcomes in the regeneration of injured skin tissues.[68] However, these procedures usually suffer from limited cell source, their storage conditions, and their viability in desired locations. These requirements necessitate the development of scalable cell production strategies, designing novel storage platforms, and utilization of new cell delivery systems.

In this study, a novel cell storage/delivery platform was developed, which showed improved cell survival and enhanced cytokine secretion. Culturing MSCs in 3D spherical shapes (i.e., spheroids) and encapsulating them into alginate microbeads was used as a solution to address the conventional challenges associated with 2D cell culture systems.[69] Cell−cell and cell−ECM interactions in spheroids closely mimic the microenvironment of cells in tissues. It was revealed that for the hanging-drop method, the optimum number of cells to form aggregates and create spheroids in the shortest period of time is approximately 8000 MSCs per drop. The spherical shapes of cells and alginate microbeads enable delivery of densely packed cells (i.e., to culture more MSCs in a relatively small volume) to the wound area, which is of crucial importance for cell-based therapies. The requirement for delivery of a high number of cells in clinical applications cannot be achieved by polymeric dressing cultured with single cells because of the low density of cells in 2D culturing systems. It was observed that the spheroid culture of MSCs significantly increases cell density and the secretion of two inhibitory cytokines, IL-10 and TGF-β1, which play pivotal roles during the wound-healing process. TGF-β1 plays a significant role in all stages of wound healing by promoting fibroblast proliferation, secretion of matrix proteins, tissue granulation, and accelerating re-epithelialization.[61] The early stage and gradual release of TGF-β1 stimulate the expression of α-SMA in fibroblasts and triggers contraction and prominent re-epithelialization of wounds dressed with alginate-encapsulated spheroids. These hydrogels act as protecting microenvironments, which enhance the viability of the stem cell while absorbing the exudates at the early stages of wound healing. Furthermore, it provides a susceptible environment for wound healing via water retention and gradual release of growth factors over time.

IL-10 is an anti-inflammatory cytokine that is essential for the regeneration of fetal wounds without leaving any scar.[70] This cytokine has pleiotropic effects, including reducing the inflammatory responses, regulation of fibroblast function, inducing hyaluronan production, and increasing vascularization.[60] Elevated levels of IL-10 secretion from encapsulated spheroids resulted in the attenuation of the inflammatory phase of wound healing. Besides, the overlapping of the inflammatory phase with proliferation of fibroblasts shortens the granulation time to 7 days. The electrospraying technique was applied to adjust the size of alginate beads to 200−300 μm while reducing the production time; i.e., it is possible to produce approximately 3500 microbeads/min when tuning the alginate flow rate at 7 mL/h. As mentioned in previous studies, the potential of hypothermic storage (at 15 °C) for alginate-encapsulated cells can greatly enhance their applications for ready-to-use and clinical applications.[46] Alginate-encapsulated cells can also be cryopreserved with minimum reduction in cell survival.[47]

The space-filling characteristic of the injectable hydrogel, before gelling, in deep wounds, which originates from its low viscosity at T < LCST, brings about comfort and close contact of the cells with damaged tissues. An important challenge in most of the wound dressings is the depth filling of the wounds and the effective delivery of cells to the wound cavities. In situ-forming thermosensitive gels behave like a low-viscosity fluid at low temperature, while at elevated temperatures (T > LCST), they form a semisolid gel. Viscous flow enables wound filling just after injection, while after the sol-to-gel transition, the hydrogel stops flowing and fixes microbeads in their locations. When the temperature increases beyond the LCST, water is released from the PNIPAm matrix because of hydrophilicity alternation, which results in hydrogel shrinkage. Blending with gelatin, which shows high water uptake characteristics, was used as a solution to prevent this adverse effect and enhance the water retention capability of the hydrogel. Moreover, gelatin improves the biodegradation properties of the hydrogel. Water retention and biodegradability features of this hydrogel make it appealing for skin tissue engineering.

Wound regeneration was significantly prominent in the S-MSC@MB-/hydrogel-treated group, which can be interpreted as a high-level secretion of cytokines (i.e., IL-10 and TGFβ1), protecting cytokines from the harsh environment of the wound, and controlled/prolonged delivery of cytokines to the wound site. The composite hydrogel absorbs and retains wound exudates in the early days after injury, inhibiting prolonged inflammation. By gradual accumulation of the mentioned secreted cytokines in the wound area, the population of myofibroblasts that express α-SMA increased, resulting in wound contraction accompanied by the creation of a thickened epithelial layer within 7 days. However, a thick layer of epithelium with disorganized deposition of collagen fibrils in the basal layer and the dermis results in scar formation in the untreated group. It was observed that α-SMA-expressing myofibroblasts disappear in the following days. It is evident that neovascularization, parallel fine collagen bundles, and reduced α-SMA in the upper layers of the skin on day 21 reduced the scar formation. It was observed that wound healing and skin regeneration for MSC@MB-/hydrogel-treated injuries were just slightly better compared to the MB-/hydrogel-treated wound, in contrast to expectations. This phenomenon can be explained by the presence of insufficient numbers of live cells in the wound area and the lack of cumulative effect observed in spheroids. Indeed, low cell density in the wound area for MSC@MB-/hydrogel-treated injuries results in reduced paracrine signaling. In this study, we designed a ready-to-use, easy-to-handle wound dressing by encapsulating cells in alginate to maintain their viability.

5. CONCLUSIONS

An injectable thermosensitive hydrogel was utilized as a wound-dressing and in situ drug-synthesis and delivery platform for wound-healing applications. MSCs and S-MSCs were encapsulated into sodium alginate microbeads using an electrospray setup to adjust the size of microbeads. The microbeads were incorporated into the thermosensitive

https://dx.doi.org/10.1021/acsbiomaterials.0c00988
ACS Biomater. Sci. Eng. XXXX, XXX, XXX−XXX

hydrogel to make a cell delivery platform. The obtained results showed that the LCST of the hydrogel is near skin temperature, which enables the filling of cavities of irregular shapes in the wound site before gelation and prevents microbead movement after sol-to-gel transition. In vitro investigations revealed that the secretion of IL-10 and TGF-β1 was greatly enhanced after encapsulation. Besides, the concentration of these cytokines was gradually increased for encapsulated cells/spheroids, while the opposite trend was observed for free cells/spheroids. In vivo investigations on a full-thickness wound model on rabbit ear showed that it took only 14 days for the wound to heal completely for the S-MSC@MB-/hydrogel-treated groups.

AUTHOR INFORMATION

Corresponding Authors

Mehrak Zare − *Skin and Stem Cell Research Center, Tehran University of Medical Sciences, Tehran, Iran*; Email: mehrakzare@gmail.com

Masoud Mozafari − *Department of Tissue Engineering & Regenerative Medicine, Faculty of Advanced Technologies in Medicine, Iran University of Medical Sciences, Tehran, Iran*; orcid.org/0000-0002-0232-352X; Email: mozafari.masoud@gmail.com, m.mozafari@utoronto.ca

Authors

Mohammad Ali Nilforoushzadeh − *Skin and Stem Cell Research Center, Tehran University of Medical Sciences, Tehran, Iran*

Mohsen Khodadadi Yazdi − *Skin and Stem Cell Research Center, Tehran University of Medical Sciences, Tehran, Iran*

Shaghayegh Baradaran Ghavami − *Basic and Molecular Epidemiology of Gastrointestinal Disorders Research Center, Research Institute for Gastroenterology and Liver Diseases, Shahid Beheshti University of Medical Sciences, Tehran, Iran*

Samila Farokhimanesh − *Department of Biotechnology, Applied Biophotonics Research Center, Science and Research Branch, Islamic Azad University, Tehran, Iran*

Leila Mohammadi Amirabad − *Marquette University School of Dentistry, Milwaukee, Wisconsin 53233, United States*; orcid.org/0000-0003-1835-4563

Payam Zarrintaj − *School of Chemical Engineering, Oklahoma State University, Stillwater, Oklahoma 74078, United States*

Mohammad Reza Saeb − *Center of Excellence in Electrochemistry, School of Chemistry, College of Science, University of Tehran, Tehran, Iran*

Michael R. Hamblin − *Wellman Center for Photomedicine, Massachusetts General Hospital, Boston, Massachusetts 02114, United States; Department of Dermatology, Harvard Medical School, Boston, Massachusetts 02115, United States; Laser Research Centre, Faculty of Health Science, University of Johannesburg, Doornfontein 2028, South Africa*; orcid.org/0000-0001-6431-4605

Complete contact information is available at: https://pubs.acs.org/10.1021/acsbiomaterials.0c00988

Notes

The authors declare no competing financial interest.

REFERENCES

(1) Eming, S. A.; Martin, P.; Tomic-Canic, M. Wound repair and regeneration: mechanisms, signaling, and translation. *Sci. Transl. Med.* **2014**, *6*, No. 265sr6.

(2) Guo, Sa.; DiPietro, L. A. Factors affecting wound healing. *J. Dent. Res.* **2010**, *89*, 219−229.

(3) Niu, Y.; Li, Q.; Ding, Y.; Dong, L.; Wang, C. Engineered delivery strategies for enhanced control of growth factor activities in wound healing. *Adv. Drug Delivery Rev.* **2019**, *146*, 190−208.

(4) Karppinen, S.-M.; Heljasvaara, R.; Gullberg, D.; Tasanen, K.; Pihlajaniemi, T. Toward understanding scarless skin wound healing and pathological scarring. *F1000Research* **2019**, *8*, No. 787.

(5) Sun, L.; Zhao, J.; Ouyang, Z.; Zeng, D. J. J. oN. M. SPION-GOx conjugate for imaging guided cancer therapy. *J. Nucl. Med.* **2019**, *60*, 1316.

(6) Walmsley, G. G.; et al. Scarless wound healing: chasing the holy grail. *Plast. Reconstr. Surg.* **2015**, *135*, 907−917.

(7) Eaton, K.; Yang, H.; Giachelli, C.; Scatena, M. Engineering macrophages to control the inflammatory response and angiogenesis. *Exp. Cell Res.* **2015**, *339*, 300−309.

(8) Wynn, T.; Vannella, K. Macrophages in Tissue Repair, Regeneration, and Fibrosis. *Immunity* **2016**, *44*, 450−462.

(9) Zhao, R.; Liang, H.; Clarke, E.; Jackson, C.; Xue, M. Inflammation in chronic wounds. *Int. J. Mol. Sci.* **2016**, *17*, No. 2085.

(10) Makrantonaki, E.; Wlaschek, M.; Scharffetter-Kochanek, K. Pathogenesis of wound healing disorders in the elderly. *JDDG: Journal der Deutschen Dermatologischen Gesellschaft* **2017**, *15*, 255−275.

(11) Leung, A.; Crombleholme, T. M.; Keswani, S. G. Fetal wound healing: implications for minimal scar formation. *Curr. Opin. Pediatr.* **2012**, *24*, 371−378.

(12) Shahbazi, M.-A.; et al. Targeted Reinforcement of Macrophage Reprogramming Toward M2 Polarization by IL-4-Loaded Hyaluronic Acid Particles. *ACS Omega* **2018**, *3*, 18444−18455.

(13) Zarrintaj, P.; et al. Can regenerative medicine and nanotechnology combine to heal wounds? The search for the ideal wound dressing. *Nanomedicine* **2017**, *12*, 2403−2422.

(14) Servatan, M.; et al. Zeolites in drug delivery: Progress, challenges and opportunities. *Drug Discovery Today* **2020**, *25*, 642−656.

(15) Yazdi, M. K.; et al. Agarose-based biomaterials for advanced drug delivery. *J. Controlled Release* **2020**, *326*, 523−543.

(16) Yazdi, M. K.; et al. Zeolites for theranostic applications. *J. Mater. Chem. B* **2020**, *8*, 5992−6012.

(17) Anjana, J.; Rajan, V. K.; Biswas, R.; Jayakumar, R. Controlled delivery of bioactive molecules for the treatment of chronic wounds. *Curr. Pharm. Des.* **2017**, *23*, 3529−3537.

(18) Chouhan, D.; Thatikonda, N.; Nilebäck, L.; Widhe, M.; Hedhammar, M.; Mandal, B. B. Recombinant spider silk functionalized silkworm silk matrices as potential bioactive wound dressings and skin grafts. *ACS Appl. Mater. Interfaces* **2018**, *10*, 23560−23572.

(19) Zarrintaj, P.; et al. Zeolite in tissue engineering: Opportunities and challenges. *MedComm* **2020**, *1*, 5−34.

(20) You, H.-J.; Han, S.-K. Cell therapy for wound healing. *J. Korean Med. Sci.* **2014**, *29*, 311−319.

(21) Kim, H. J.; Park, J.-S. Usage of human mesenchymal stem cells in cell-based therapy: advantages and disadvantages. *Dev. Reprod.* **2017**, *21*, 1.

(22) Abbasi-Malati, Z.; Roushandeh, A. M.; Kuwahara, Y.; Roudkenar, M. H. Mesenchymal stem cells on horizon: a new arsenal of therapeutic agents. *Stem Cell Rev. Rep.* **2018**, *14*, 484−499.

(23) Bagheri, B.; et al. Tissue engineering with electrospun electroresponsive chitosan-aniline oligomer/polyvinyl alcohol. *Int. J. Biol. Macromol.* **2020**, *147*, 160−169.

(24) Khalili, R.; Zarrintaj, P.; Jafari, S. H.; Vahabi, H.; Saeb, M. R. Electroactive poly (p-phenylene sulfide)/r-Graphene Oxide/Chitosan as a novel potential candidate for tissue engineering. *Int. J. Biol. Macromol.* **2020**, *154*, 18−24.

https://dx.doi.org/10.1021/acsbiomaterials.0c00988
ACS Biomater. Sci. Eng. XXXX, XXX, XXX−XXX

(25) Han, Y.; Li, X.; Zhang, Y.; Han, Y.; Chang, F.; Ding, J. Mesenchymal stem cells for regenerative medicine. *Cells* **2019**, *8*, No. 886.
(26) Amirkhani, M. A.; Zare, S.; Shoaei-Hassani, A.; Torbati, E.; Nilforoushzadeh, M. A. Literature Review of Adipose-derived Mesanchymal Cells from History to Approaches. *Iran Red Crescent Med. J.* **2017**, *19*, No. e22940.
(27) Wang, L.; et al. Exosomes secreted by human adipose mesenchymal stem cells promote scarless cutaneous repair by regulating extracellular matrix remodelling. *Sci. Rep.* **2017**, *7*, No. 13321.
(28) Smith, A. N.; et al. Mesenchymal stem cells induce dermal fibroblast responses to injury. *Exp. Cell Res.* **2010**, *316*, 48−54.
(29) Kato, J.; et al. Mesenchymal stem cells ameliorate impaired wound healing through enhancing keratinocyte functions in diabetic foot ulcerations on the plantar skin of rats. *J. Diabetes Complications* **2014**, *28*, 588−595.
(30) Costa, M. H.; McDevitt, T. C.; Cabral, J. M.; da Silva, C. L.; Ferreira, F. C. Tridimensional configurations of human mesenchymal stem/stromal cells to enhance cell paracrine potential towards wound healing processes. *J. Biotechnol.* **2017**, *262*, 28−39.
(31) Petrenko, Y.; Syková, E.; Kubinová, Š. The therapeutic potential of three-dimensional multipotent mesenchymal stromal cell spheroids. *Stem Cell Res. Ther.* **2017**, *8*, No. 94.
(32) Wang, M.; Yuan, Q.; Xie, L. Mesenchymal stem cell-based immunomodulation: properties and clinical application. *Stem Cells Int.* **2018**, *2018*, No. 3057624.
(33) Lee, D. E.; Ayoub, N.; Agrawal, D. K. Mesenchymal stem cells and cutaneous wound healing: novel methods to increase cell delivery and therapeutic efficacy. *Stem Cell Res. Ther.* **2016**, *7*, No. 37.
(34) Farokhimanesh, S.; Nilforoushzade, M. A.; Nikkhah, N.; Komeili, A.; Zare, M. Scarless Wound Healing: Looking for a Single Remedy With Multiple Targets. *J. Skin Stem Cell* **2017**, *4*, No. e67299.
(35) Hu, M. S.; Borrelli, M. R.; Lorenz, H. P.; Longaker, M. T.; Wan, D. C. Mesenchymal stromal cells and cutaneous wound healing: a comprehensive review of the background, role, and therapeutic potential. *Stem Cells Int.* **2018**, *2018*, No. 6901983.
(36) Ryu, N.-E.; Lee, S.-H.; Park, H. Spheroid Culture System Methods and Applications for Mesenchymal Stem Cells. *Cells* **2019**, *8*, 1620.
(37) Mizukami, A.; et al. Priming approaches to improve the efficacy of mesenchymal stromal cell-based therapies. *Stem Cell Res. Ther.* **2019**, *10*, No. 131.
(38) Zare, M.; Soleimani, M.; Mohammadian, M.; Akbarzadeh, A.; Havasi, P.; Zarghami, N. Efficient biotechnological approach for lentiviral transduction of induced pluripotent stem cells. *Artif. Cells, Nanomed., Biotechnol.* **2016**, *44*, 743−748.
(39) Cesarz, Z.; Tamama, K. Spheroid culture of mesenchymal stem cells. *Stem Cells Int.* **2016**, *2016*, No. 9176357.
(40) Tran, C.; Damaser, M. S. Stem cells as drug delivery methods: application of stem cell secretome for regeneration. *Adv. Drug Delivery Rev.* **2015**, *82*, 1−11.
(41) Yildirimer, L.; Thanh, N. T.; Seifalian, A. M. Skin regeneration scaffolds: a multimodal bottom-up approach. *Trends Biotechnol.* **2012**, *30*, 638−648.
(42) Chouhan, D.; Dey, N.; Bhardwaj, N.; Mandal, B. B. Emerging and innovative approaches for wound healing and skin regeneration: current status and advances. *Biomaterials* **2019**, *216*, No. 119267.
(43) Andersen, T.; Auk-Emblem, P.; Dornish, M. 3D cell culture in alginate hydrogels. *Microarrays* **2015**, *4*, 133−161.
(44) Alizadeh, R.; et al. Conductive hydrogels based on agarose/alginate/chitosan for neural disorder therapy. *Carbohydr. Polym.* **2019**, *224*, No. 115161.
(45) Atoufi, Z.; Zarrintaj, P.; Motlagh, G. H.; Amiri, A.; Bagher, Z.; Kamrava, S. K. Polymer edition, "A novel bio electro active alginate-aniline tetramer/agarose scaffold for tissue engineering: synthesis, characterization, drug release and cell culture study. *J. Biomater. Sci., Polym. Ed.* **2017**, *28*, 1617−1638.
(46) Swioklo, S.; Constantinescu, A.; Connon, C. J. Alginate-encapsulation for the improved hypothermic preservation of human adipose-derived stem cells. *Stem Cells Transl. Med.* **2016**, *5*, 339−349.
(47) Benson, E. E.; Harding, K.; Ryan, M.; Petrenko, A.; Petrenko, Y.; Fuller, B. Alginate Encapsulation to Enhance Biopreservation Scope and Success: A Multidisciplinary Review of Current Ideas and Applications in Cryopreservation and Non-Freezing Storage," (in eng). *CryoLetters* **2018**, *39*, 14−38.
(48) Ho, S. S.; Murphy, K. C.; Binder, B. Y.; Vissers, C. B.; Leach, J. K. Increased survival and function of mesenchymal stem cell spheroids entrapped in instructive alginate hydrogels. *Stem Cells Transl. Med.* **2016**, *5*, 773−781.
(49) Yazdi, M. K.; et al. Agarose-based biomaterials for advanced drug delivery. *J. Controlled Release* **2020**, *326*, 523−543.
(50) Zarrintaj, P.; et al. Poloxamer: A versatile tri-block copolymer for biomedical applications. *Acta Biomater.* **2020**, *110*, 37−67.
(51) Salati, M. A.; et al. Agarose-Based Biomaterials: Opportunities and Challenges in Cartilage Tissue Engineering. *Polymers* **2020**, *2*, No. 1150.
(52) Zarrintaj, P.; et al. Agarose-based biomaterials for tissue engineering. *Carbohydr. Polym.* **2018**, *187*, 66−84.
(53) Zarrintaj, P.; et al. Thermo-sensitive polymers in medicine: A review. *Eur. Polym. J.* **2019**, *117*, 402−423.
(54) Blacklow, S.; Li, J.; Freedman, B.; Zeidi, M.; Chen, C.; Mooney, D. Bioinspired mechanically active adhesive dressings to accelerate wound closure. *Sci. Adv.* **2019**, *5*, No. eaaw3963.
(55) Bagher, Z.; et al. Conductive hydrogel based on chitosan-aniline pentamer/gelatin/agarose significantly promoted motor neuron-like cells differentiation of human olfactory ecto-mesenchymal stem cells. *Mater. Sci. Eng., C* **2019**, *101*, 243−253.
(56) Chen, S.; et al. Study of stiffness effects of poly (amidoamine)−poly (N-isopropyl acrylamide) hydrogel on wound healing. *Colloids Surf., B* **2016**, *140*, 574−582.
(57) Shi, J.-H.; et al. Protection against TGF-β1-induced fibrosis effects of IL-10 on dermal fibroblasts and its potential therapeutics for the reduction of skin scarring. *Arch. Dermatol. Res.* **2013**, *305*, 341−352.
(58) Sapudom, J.; Wu, X.; Chkolnikov, M.; Ansorge, M.; Anderegg, U.; Pompe, T. Fibroblast fate regulation by time dependent TGF-β1 and IL-10 stimulation in biomimetic 3D matrices. *Biomater. Sci.* **2017**, *5*, 1858−1867.
(59) Harrell, C. R.; Fellabaum, C.; Jovicic, N.; Djonov, V.; Arsenijevic, N.; Volarevic, V. Molecular mechanisms responsible for therapeutic potential of mesenchymal stem cell-derived secretome. *Cells* **2019**, *8*, No. 467.
(60) Steen, E. H.; Wang, X.; Balaji, S.; Butte, M. J.; Bollyky, P. L.; Keswani, S. G. the role of the anti-inflammatory cytokine interleukin-10 in tissue fibrosis. *Adv. Wound Care* **2020**, *9*, 184−198.
(61) Pakyari, M.; Farrokhi, A.; Maharlooei, M. K.; Ghahary, A. Critical role of transforming growth factor beta in different phases of wound healing. *Adv. Wound Care* **2013**, *2*, 215−224.
(62) Vossoughi, A.; Matthew, H. W. Encapsulation of mesenchymal stem cells in glycosaminoglycans-chitosan polyelectrolyte microcapsules using electrospraying technique: Investigating capsule morphology and cell viability. *Bioeng. Transl. Med.* **2018**, *3*, 265−274.
(63) Yazdi, M. K.; et al. Hydrogel membranes: A review. *Mater. Sci. Eng., C* **2020**, *114*, No. 111023.
(64) Vorwald, C. E.; Ho, S. S.; Whitehead, J.; Leach, J. K. High-throughput formation of mesenchymal stem cell spheroids and entrapment in alginate hydrogels. In *Methods in Molecular Biology*; Springer, 2018; Vol. *1758*, pp 139−149.
(65) Lee, G. M.; Han, B. K.; Kim, J. H.; Palsson, B. O. Effect of calcium chloride treatment on hybridoma cell viability and growth. *Biotechnol. Lett.* **1992**, *14*, 891−896.
(66) Riffle, S.; Hegde, R. S. Modeling tumor cell adaptations to hypoxia in multicellular tumor spheroids. *J. Exp. Clin. Cancer Res.* **2017**, *36*, No. 102.
(67) Shinde, A. V.; Humeres, C.; Frangogiannis, N. G. The role of α-smooth muscle actin in fibroblast-mediated matrix contraction and

https://dx.doi.org/10.1021/acsbiomaterials.0c00988
ACS Biomater. Sci. Eng. XXXX, XXX, XXX−XXX

remodeling. *Biochim. Biophys. Acta, Mol. Basis Dis.* **2017**, *1863*, 298−309.
(68) Kabat, M.; Bobkov, I.; Kumar, S.; Grumet, M. Trends in mesenchymal stem cell clinical trials 2004-2018: Is efficacy optimal in a narrow dose range? *Stem Cells Transl. Med.* **2020**, *9*, 17−27.
(69) Mirbagheri, M.; Adibnia, V.; Hughes, B. R.; Waldman, S. D.; Banquy, X.; Hwang, D. K. Advanced cell culture platforms: a growing quest for emulating natural tissues. *Mater. Horiz.* **2019**, *6*, 45−71.
(70) Peranteau, W. H.; et al. IL-10 overexpression decreases inflammatory mediators and promotes regenerative healing in an adult model of scar formation. *J. Invest. Dermatol.* **2008**, *128*, 1852−1860.

https://dx.doi.org/10.1021/acsbiomaterials.0c00988
ACS Biomater. Sci. Eng. XXXX, XXX, XXX−XXX